Desalination and Water Treatment
www.deswater.com

doi: 10.5004/dwt.2017.0253

60 (2017) 170–179
January

Removal of Ponceau S by adsorption onto alumino-phosphate: efficiency and modeling

Abdenacer Flilissa[a,*], Widad Sebaihi[a], Venkataraman Sivasankar[b], Mokhtar Boutahala[c], André Darchen[d]

[a]*Laboratoire des maladies Cardiovasculaire, Génétiques et Nutritionnelles, Département de Pharmacie, Faculté de Médecine, Université Ferhat Abbas, Sétif-1, 19000, Algeria, Tel. +213 777156810; email: konicakp34@yahoo.fr*
[b]*Department of Civil Engineering, School of Engineering, Nagasaki University, Nagasaki-Daigaku, 1-14 Bunkyo-machi, Nagasaki 852 8521, Japan, email: sivshri.20@gmail.com*
[c]*Laboratoire de Génie des Procédés Chimiques, Département de Génie des Procédés, Faculté de Technologie, Université Ferhat Abbas, Sétif-1, 19000, Algeria, email: mboutahala@yahoo.fr*
[d]*UMR CNRS 6226 Institut des Sciences Chimiques de Rennes, ENSCR, 11 Allée de Beaulieu, CS 50837, 35708, Rennes Cedex 7, France, email: Andre.Darchen@ensc-rennes.fr*

Received 6 March 2016; Accepted 13 June 2016

ABSTRACT

Ponceau S (PS) is an azo dye widely used for versatile applications in foods and biochemistry; nevertheless, it is suspected to be toxic and carcinogenic. In this research article, the removal of PS from aqueous solution was investigated by adsorption onto alumino-phosphate ($AlPO_4$). This adsorbent has been synthesized by precipitation from solution of aluminum salt. It was an amorphous solid with a specific area and pH_{zpc} of 100 m^2/g and 4.6, respectively. The efficiency of PS sorption as a function of pH, initial PS concentration, $AlPO_4$ dose and temperature was studied. The present PS sorption dynamics followed the pseudo-first-order model and the calculated sorption capacity was in good agreement with the experimental values. The compliance of isotherm models such as Langmuir, Freundlich and Sips was also verified. Among the isotherm models, Sips was deemed to be the better fit than others. PS sorption as a function of temperature explicates an exothermic nature of sorption which decreased from 9.12 mg g^{-1} (300 K) to 6.08 mg g^{-1} (315 K). The adsorbed PS on $AlPO_4$ was easily desorbed by washing at pH 7 and the adsorption equilibrium was established in the first 8 min. The PS laden adsorbent was also regenerated by heating at 600°C for 30 min and the regenerated $AlPO_4$ was attempted for its continual utilization for the adsorption of PS successfully.

Keywords: Ponceau S; $AlPO_4$; Adsorption; Desorption; Regeneration

1. Introduction

Dyes are synthetic and complex molecular structures which are stable and difficult to biodegrade [1, 2]. Azo dyes constitute the largest group of compounds responsible for water pollution worldwide. Synthetic azo dyes are widely used in textile, printing, cosmetic, food colorants and pharmaceutical industries, and they are also important in laboratories as biological stains or pH indicators. The presence of synthetic azo dyes in wastewaters is not only esthetically unpleasant but also harmful due to their carcinogenic and mutagenic properties [3–6]. Therefore, these dyes need to be removed from wastewaters before discharging them into the environment. The red colored anionic azo dye Ponceau S (PS) (or Acid Red 112) is widely used in leather tanning processes [7]. To a less extent, it is also used in a variety of application fields such as paints, inks and plastics. PS is also used to prepare a stain for rapid reversible detection of protein bands on nitrocellulose or PVDF membranes

* Corresponding author.

(Western blotting) [8]. However, its biotransformation products have toxic effects against aquatic organisms and became suspicious of being carcinogenic for humans [8]. PS may elicit intolerance in people allergic to salicylates (aspirin) and it is a histamine liberator, and may intensify symptoms of asthma [9].

There are numerous methods for the removal of synthetic azo dyes from aqueous solutions, such as coagulation and flocculation [10, 11], ozone assisted electrocoagulation [12, 13], biodegradation [14], economical biomaterial [15], adsorption onto layered double hydroxides (LDH) [16], and Advanced Oxidation Processes (AOPs) [17]. The adsorption has been proved to be one of the most promising techniques due to its easy operations, high capacity in many applications, fast kinetics, and mild regeneration conditions [18]. Indeed, very few researchers have worked on the removal of PS. Meena et al. showed nearly complete decolorization of PS in the presence of methylene blue immobilized resin Dowex-11 photocatalyst [19]. PS is also removed by photocatalysis process and adsorption on nano-sized ZnO [20]. Shin and Chae [21] used organic clay to remove PS through adsorption study. In continuation to this work, El-Desoky et al. [22] attempted electrochemical degradation and decolorization of PS dye with an achievement of 98% mineralization. Degradation of PS dye using photo-catalytic materials such as nano-sized niobium pentoxide with carbon [23], nano-structured Ni-doped TiO_2 [9] and zinc oxide [24] was also favorably performed. Sahoo et al. [25] attempted PS removal by UVC induction in the presence of oxidants and by Fenton-Fenton like processes [26]. Deng and his coworkers [27] studied the quick adsorption of PS dye by PVA@$SiO_{1.5}$ – hPEA gels with high adsorption capacity. The adsorption of the PS occurs on MgO nanoparticles [28], charcoal ash [29], chitin [30] and ZnS nanoparticles [31]. In addition, few biological methods have also been reported for the decolorization of PS in aqueous solutions [32, 33]. However, the microbial degradation was reported to be inefficient due to the low and incomplete decolorization/degradation [34]. Fenton and Fenton-like processes were also used in the mineralization of PS, but the treated solutions were found to be more biotoxic than those containing the original dyes [35]. In the recent past, many researchers carried out studies on the removal PS dye by adopting various techniques [36, 37]. Presently, hierarchial organic–inorganic hybrid nanofibrous membrane was able to capture 96% of PS dye within a short time of 20 min as reported by Li et al. [38].

Alumino-phosphates' (AlO_4-PO_4) present interest exhibits a diverse stoichiometries, wealthy structural features and fascinating chemical architectures due to exhaustive co-ordinations of Al and P atoms. These are typically built from strict alternation of AlO_4 and PO_4 tetrahedra shared through corners to form a neutral open framework. Aluminophosphate structures are made up of Al-centered polyhedral (AlO_4, AlO_5, AlO_6) and P-centered tetrahedral $P(O_b)_n$ $(O_t)_{4-n}$ (b = bridging; t = terminal; n = 1, 2, 3, 4). Hu and Xu [39] elaborately discussed the rich structural chemistry of alumino-phosphates. In a recent paper, the removal of cetylpyridinium by electrocoagulation shows that $AlPO_4$ and phosphate modified alumina can adsorb more efficiently than alumina [40]. This result gave us the opportunity to investigate the use of $AlPO_4$ in the removal of a dye from aqueous solutions.

According to the literature review, the $AlPO_4$ has not been used so far as adsorbent in the PS removal. In the present study, the removal of PS from aqueous solution has been studied using batch experiments and the pH effect. The contact time and the temperature have also been investigated. The isotherm studies were carried out using Langmuir, Freundlich and Sips models.

2. Materials and methods

2.1. Chemicals

The anionic diazo dye PS (Acid Red 112; CI 27195; IUPAC name: 3-Hydroxy-4-(2-sulfo-4-[4-sulfophenylazo] phenylazo)-2,7-naphthalenedisulfonic acid sodium salt (Fig. 1) with the molecular formula $C_{22}H_{12}N_4Na_4O_{13}S_4$ was supplied by Sigma-Aldrich, Germany. Analytical reagent grade samples of aluminum chloride ($AlCl_3.6H_2O$, 99%) and phosphoric acid (H_3PO_4, 99%) were supplied by Sigma-Aldrich. All other chemical reagents were commercial and used without further purification. All aqueous solutions were prepared by dissolution in de-ionized water.

2.2. Synthesis of $AlPO_4$

Synthesis of alumino-phosphate, $AlPO_4$, was performed by precipitation method [41]. Exactly, 12.99 g of $AlCl_3.6H_2O$ in 300 mL of de-ionized water was dissolved and to which 3.57 mL of H_3PO_4 was added in drop wise under a stirring agitation. The pH was increased to 5 at the end of precipitation by the addition of 0.5 M NaOH. As a result, the turbidity increased sharply, showing the formation of a white solid which was then filtered, washed with de-ionized water and finally vacuum dried in oven at 80°C for 24 h. The dry mass of 15 g of $AlPO_4$ was obtained.

2.3. Analysis

The concentration of PS was measured using UV/visible spectrophotometer (PerkinElmer Lambda 35) at λ_{max} = 521 nm. The FT-IR spectra were recorded on a Shimadzu spectrometer using samples as solid (KBr disks). Powder X-ray diffraction (XRD) patterns were recorded with a INEL XRG 3.500 diffractometer using CuKα (1.540560 Å) at 30 kV and 30 mA with an

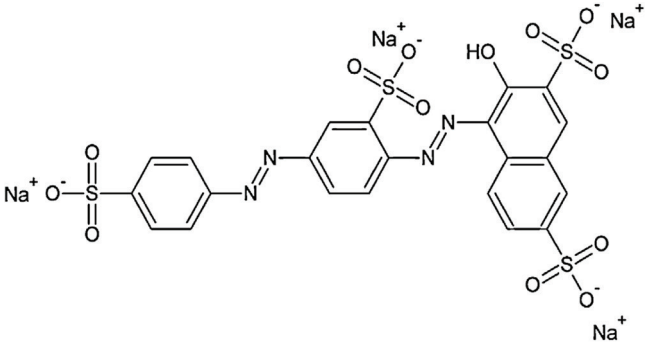

Fig. 1. Molecular structure of Ponceau S (PS).

angle range 2θ between 5° and 120° and step length of 0.02° (2θ). The specific area of $AlPO_4$ was determined by the model of Brunauer, Emmett and Teller (BET method). The pH was measured using a pH-meter Metrohm 827.

2.4. Determination of pH of zero charge (PZC)

The pH_{zpc} of $AlPO_4$ was determined by the pH drift method [42]. For this purpose, 0.05 L of a 0.01 M $NaNO_3$ solution was placed in a jacketed titration vessel, thermostated at 298 K, and N_2 was bubbled through the solution to stabilize the pH by preventing the dissolution of CO_2. The pH was then adjusted to successive initial values between 2 and 12, by adding either HCl or NaOH and the $AlPO_4$ (0.1 g) was added to the solution. The final pH, reached after 48 h, was measured and plotted against the initial pH. The pH at which the final pH crosses the line $pH_{final} = pH_{initial}$ is taken as the pH_{PZC} of the given $AlPO_4$.

2.5. Adsorption and desorption experiments

The influence of the pH on PS adsorption onto $AlPO_4$ was investigated in the pH range of 2–10. The suspensions containing 0.2 g of $AlPO_4$ in 50 mL PS solutions of 0.03 and 0.05 mmol/L were stirred at 22 ± 1°C for 200 min. They were then centrifuged at 4,000 rpm for 10 min and the PS concentration was estimated spectrophotometrically at λ_{max} of 521 nm.

For the kinetic and isotherm studies, 50 mL of PS solution at different concentrations (0.03 mmol/L, 0.05 mmol/L, 0.07 mmol/L and 0.09 mmol/L) were continuously stirred at 200 rpm in the presence of 0.2 g of $AlPO_4$ at 22 ± 1°C and pH 2.55. Then, the PS was estimated.

At first, the PS loaded adsorbents were prepared by the adsorption of PS on 0.2 g of $AlPO_4$ in 50 mL of 0.03 and 0.05 mM PS solutions at pH 2.55. The pH effect on desorption was performed by addition of 0.5 M NaOH in order to obtain the pH range of 2.55–8.00. For each pH value, the solution was stirred for 50 min before analysis. The amount of the PS desorbed from $AlPO_4$ was determined using experimental equation: $q_{des} = CV/m$, where C (mol/L) is the PS concentration in solution, V (L) volume solution and m (g) is the mass of the adsorbent. The regeneration of the PS loaded adsorbent was realized by two methods. One was realized by treating the wet adsorbent in a solution at pH 7 for 50 min and the second method was performed by heating the dry adsorbent at 600°C for 30 min.

3. Results and discussion

3.1. Characterization of $AlPO_4$

The specific surface area of the solid was determined by BET method giving 100 m^2/g. The XRD analysis of the $AlPO_4$ showed an amorphous structure (figure not shown). The IR spectrum of the solid (Fig. 2) showed an absorption band at 1,097 cm^{-1} attributed to PO_4^{3-} (P–O). The strong peak at 3,404 cm^{-1} was corresponding to the O-H stretching. Another strong and sharp peak with a maximum of 1,649 cm^{-1} was due to water molecule and a bending vibration at 523 cm^{-1} attributed to PO_4^{3-} according to the analysis of Devamani et al. [43]. The absence of bands at approximately 1,120 and 611 cm^{-1} indicates the presence of nano crystalline $AlPO_4$ [43] confirming the result given by XRD (amorphous structure). The IR spectrum of the PS adsorbed $AlPO_4$ shows an absorption band at 1,097 cm^{-1} attributed to PO_4^{3}. The peaks between 1,500 and 1,900 cm^{-1} are assignments of azo functional groups adsorbed onto PS. The band at 1,557 cm^{-1} was significant and corresponds to the function N=N. The peak which is observed at 1,404 cm^{-1} is attributed to the aromatic C=C [10] attributing the PS dye molecule. The above explanations evidenced the presence of the adsorbed PS onto $AlPO_4$.

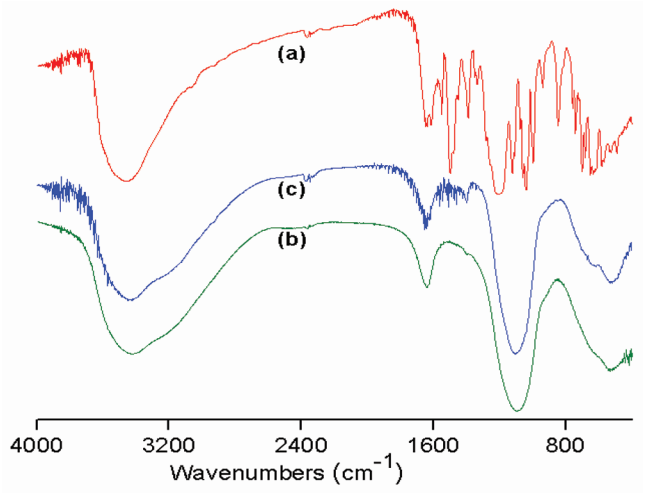

Fig. 2. IR spectrum of (a) PS pure, (b) APO_4 before and (c) after adsorption of PS.

3.2. PZC determination

A plot of the difference in the pH values (ΔpH) between pH_f and pH_i vs. pH_i provides the PZC of the $AlPO_4$ was found to be equal to 4.6 (figure not shown). This result is in agreement with the literature value which shows an increase with activation from 3.45 to 5.10 leading to a decrease in the surface acidity [44].

3.3. Effect of the pH

The effect of the pH on the removal of PS through two initial concentrations (0.03 mmol/L and 0.05 mmol/L) at different initial pH values ranging from 2 to 10 was performed with 0.2 g of adsorbent (Fig. 3). The adsorption of PS onto $AlPO_4$ decreased gradually from pH 2 to 3.5 followed by a sharp decrease from pH 3.5 to 7.0. Then, PS sorption increased till pH value reaches 10. The removal efficiency was found to be highly dependent on the pH of the PS solution. The highest efficiency of the adsorption was estimated about 97.5 ± 0.5% at pH below 4 and then it decreases. This pH range has been chosen for subsequent studies. The evolution of the adsorption in the investigated pH range is explained by the fact that when the pH is below PZC, the adsorbent $AlPO_4$ is positively charged while the PS molecule is negatively charged due to the presence of four SO_3^- groups. The adsorption may be associated with an electrostatic interaction between the negative sulfonic groups of PS and the positive charges on the surface of $AlPO_4$ [27].

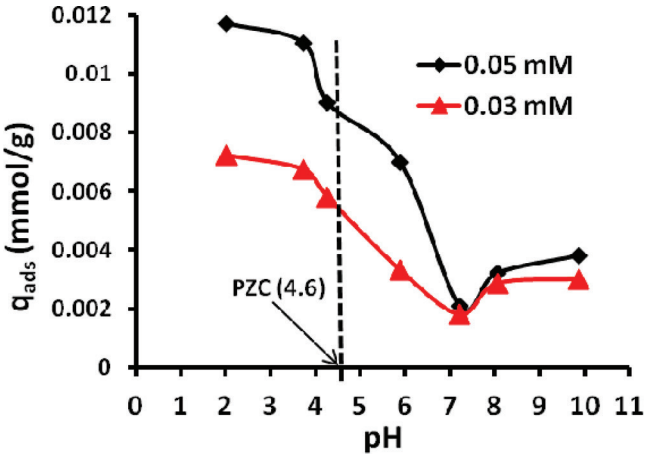

Fig. 3. Effect of pH on the adsorption of PS (0.03 and 0.05 mM) onto 0.2 g of $AlPO_4$ in 50 ml, stirring speed = 200 rpm; T = 22 ± 1°C.

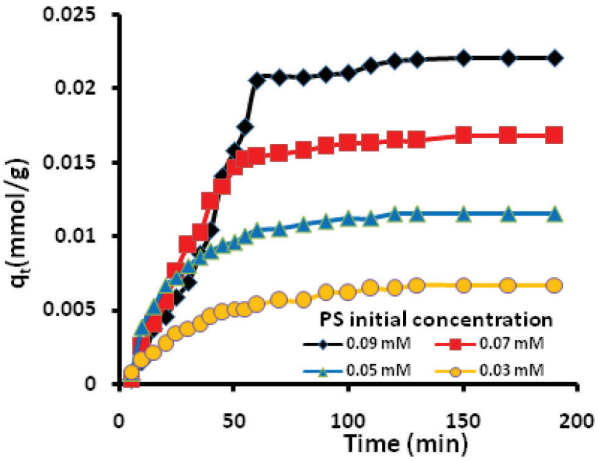

Fig. 4. Adsorption kinetics of PS onto 0.2 g $AlPO_4$ in 50 mL at pH 2.55; T = 22 ± 1°C.

3.4. Effect of temperature on PS removal

The effect of the temperature on the PS adsorption was investigated in the range 27°C–42°C. A 50-mL mixture of a solution 0.05 mmol/L PS was stirred with 0.2 g of $AlPO_4$ in a gradually heating. The adsorption amount of PS onto $AlPO_4$ decreased from 0.012 mmol/g (9.12 mg g^{-1}) to 0.008 mmol/g (6.08 mg g^{-1}) while the temperature was increased. The decrease in uptake with the temperature indicated that the sorption of the PS by $AlPO_4$ was an exothermic process similar to that of the azo dyes obtained on charcoal ash [28]. Conversely, the nature of PS sorption onto MgO nano particles almost in the same range was endothermic as reported by Venkatesha et al. [27]. This reciprocating thermodynamic nature of PS sorption brings certain decisive factors into limelight which includes pH of the PS dye solution and surface chemistry of $AlPO_4$ and MgO-nanoparticles.

3.5. Adsorption kinetics of the PS on $AlPO_4$

3.5.1. Effect of contact time

The optimization of time for the establishment of equilibrium state at different concentration of PS was initially explored. It is well depicted that the sorption of PS onto chemically synthesized $AlPO_4$ increased with respect to time. The equilibrium was reached after 50 min, indicating a rapid process of PS sorption onto $AlPO_4$. This initial rapid uptake can be attributed to the synergy between the structural features and the multifunctional adsorption elements such as tetrahedral AlO_4 and PO_4 present in $AlPO_4$. Taking the previous literatures into account, it could be corroborated that the equilibrium time of PS sorption onto $AlPO_4$ is much faster than that of ZnO, MgO, and PDA/PEI@FeCNF50 [19, 27, 38]. The $AlPO_4$ particles are likely to capture the PS molecules with a low diffusion resistance which facilitates high sorption capacity of PS molecules [45]. Additionally, the sorption performance may be ascertained due to the existing electrostatic attraction between AlO_4 tetrahedral units and anionic dye molecules as studied in the case of FeO_x with PS molecules [38]. Nevertheless, it seems quite obvious that the sorption of PS onto $AlPO_4$ particles could be rooted through high affinity between positively charged adsorbent surface and negatively charged PS species. Furthermore, the interaction of hydrogen bonding developed on the surface of $AlPO_4$ and p – p stacking of aromatic rings is envisaged for the effective capture of PS [46, 47].

3.5.2. Effect of initial PS concentrations

The adsorbed amount of PS increased with the increase of the initial concentration (Fig. 4). Hence, the adsorption of PS was favored at high concentrations. When the PS concentration was low, it only adsorbed on the surface to form a monolayer for a very short time. But when the initial concentration increased, it adsorbed to the surface and then it is seeping into the pores and the micropores of the surface of the material $AlPO_4$ required more time. This type of direct relationship between percentage removal of PS and initial concentration of PS may be attributed to the increase in driving force as a consequence of concentration gradient which could be able to overcome the mass transfer resistance of PS molecules between aqueous and solid phases. Similar observation was reported by Abbas and Trari [48] and Zhu et al. [49] using azo type of Congo red and Ponceau 4R dye molecules.

3.6. Modeling the adsorption kinetics

The pseudo-first-order, pseudo-second-order, intraparticle diffusion and Elovich models were employed to understand their compliance with the dynamics of PS sorption onto $AlPO_4$ and the kinetic parameters are presented in Table 1.

The pseudo-first-order rate equation was given by Lagergren [50] (Eq. (1)), where q_e and q_t are the amounts of dye adsorbed (mmol/g) at equilibrium and at time t (min), respectively, and k_1 (min^{-1}) is the pseudo-first-order rate constant. Values of k_1 were calculated from the plot of log ($q_e - q_t$) vs. t.

$$\log\left(q_e - q_t\right) = \log q_e - \frac{k_1}{2.303}t \quad (1)$$

Table 1
Kinetic parameters for the removal of PS on alumino-phosphate at different initial PS concentrations

Models	Parameters	Initial concentration			
		0.3	0.5	0.7	0.9
Pseudo-first-order	$q_{e,cal}$ (mmol/g) 10^4	66	103	179	419
$\log(q_e - q_t) = \log q_e - \frac{k_1}{2.303}t$	k_1 (g/mmol.min) 10^3	25.3	32.2	34.5	41.4
	R^2	0.98	0.99	0.96	0.95
Pseudo-second-order	$q_{e,cal}$ (mmol/g) 10^4	84	139	221	392
$\frac{t}{q_t} = \frac{1}{k_2 q_e^2} + \frac{1}{q_e}$	k_2 (g/mmol.min)	3.17	2.50	1.07	0.25
	R^2	0.99	0.92	0.93	0.72
Elovich	α (mmol/g min) 10^2	0.01	0.07	0.10	0.07
$q_t = \left(\frac{1}{\beta}\right)\ln(\alpha\beta) + \left(\frac{1}{\beta}\right)\ln(t)$	β (g/mmol)	1000	500	200	143
	R^2	0.98	0.94	0.92	0.90
Intra-particle diffusion (Step 2)	K_d (mmol/g $min^{0.5}$) 10^3	0.70	0.90	1.60	3.10
$q_t = k_d t^{0.5} + C$	C (mmol/g) 10^3	0.90	3.20	2.50	6.0
	R^2	0.95	0.96	0.80	0.73
Experimental data	$q_{e,exp}$ (mmol/g) 10^4	67	115	168	221

Pseudo-first-order plot (Fig. 5) for adsorption of PS onto the surface of $AlPO_4$ at different initial PS concentrations. On increasing the initial PS concentration, the equilibrium sorption capacity ($q_{e,cal}$) and the pseudo-first-order rate constant (from Eq. (1)) increases from 66.10^{-4} mmol g^{-1} to 419.10^{-4} mmol g^{-1} and 25.3×10^{-3} to 41.4×10^{-3} g/mmol.min, respectively (Table 1). The experimental ($q_{e,exp}$) data are fairly in good agreement with the calculated values ($q_{e,calc}$) obtained from the pseudo-first-order model with good R^2 values ranges from 0.99 to 0.95.

The rate equation for the pseudo-second-order model [51] is given by Eq. (2).

$$\frac{t}{q_t} = \frac{1}{k_2 q_e^2} + \frac{1}{q_e} \quad (2)$$

where k_2 (g/mg min) is the pseudo-second-order rate constant and its value was obtained from the plot of t/q_t vs. t. An increase in the pseudo-second-order rate constant was registered about 13 folds when the concentration of PS was 0.3 mmol L^{-1} when compared with the value of 0.245 g/mmol. min at 0.9 mmol L^{-1} (greater by three folds in PS concentration). It may be decisive that the initial PS concentration and pseudo-second-order rate constant are inversely proportional to each other. The R^2 values ranged from 0.99 to 0.72 and the experimental ($q_{e,exp}$) values did not match with the calculated ones ($q_{e,calc}$).

On making comparison for the fit of pseudo-first and pseudo-second order models, it can be suggested that the former fits very well and quite decisive when compared with the later.

The adsorption kinetics is generally controlled by different mechanisms. In the batch mode adsorption process, the initial adsorption occurs on the surface of the adsorbent. In addition, there is a possibility of the adsorbate to diffuse into the interior pores of the adsorbent. Weber and Morris [52] have suggested the following kinetic model to investigate whether the adsorption is intra-particle diffusion or not, according to this theory expressed in Eq. (3).

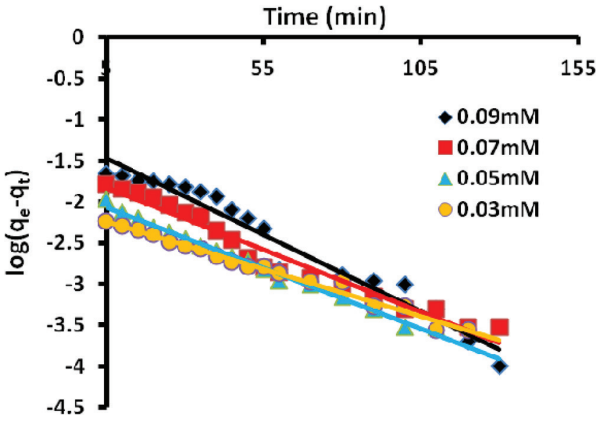

Fig. 5. Pseudo-first-order plots for the effect of initial PS concentration (mM) on the PS sorption onto 0.2 g of $AlPO_4$ at a stirring speed = 200 rpm; pH 2.55; T = 22 ± 1°C.

$$q_t = k_d t^{0.5} + C \quad (3)$$

where, k_d (mmol/g $min^{0.5}$) is the intra-particle diffusion rate constant and it is calculated by plotting q_t vs. $t^{0.5}$ and C is the value of intercept of the plot of q_t against $t^{0.5}$.

The intra-particle diffusion curves (Fig. 6) explicated the sorption of PS onto $AlPO_4$ in several steps. It was observed that the distribution of the PS on the surface of $AlPO_4$ occurs in three linear steps. The transfer of the PS from the bulk to the boundary layer surrounding the surface of the adsorbent particle and then to the adsorbents sites (Step 1) which was completed before 36 min. The diffusion in the micro and macro pores causes interactions between PS molecules and the active sites of $AlPO_4$ (Step 2) from 36 to 80 min, where intra-particle diffusion was rate controlling. The third step was attributed to the adsorption state (equilibrium stage) in which intra-particle diffusion started to slow down due to the decrease of the PS concentration in the solution. The linear

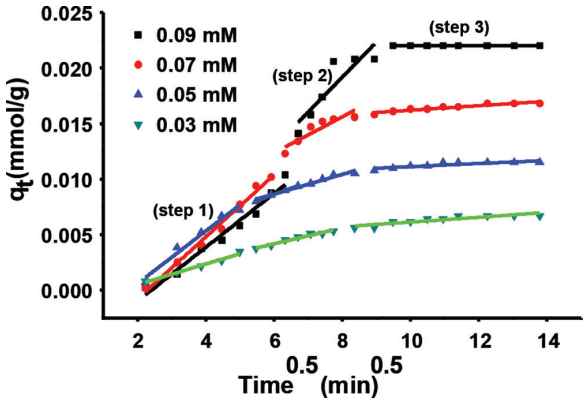

Fig. 6. Intra-particle diffusion plots of the kinetic data for PS onto 0.2 g of $AlPO_4$ at different concentrations, pH 2.55; T = 22 ± 1°C.

portion of the plot for wide range of contact time between adsorbent and adsorbate does not pass through the origin. This deviation from the origin or near saturation may be due to the variation of the mass transfer in the initial and final stages of the adsorption [53]. Such deviation from the origin indicates that pore diffusion is the only controlling step and not the film diffusion. The K_d values increased from 0.70 mmol (g $min^{0.5}$)$^{-1}$ to 3.10 mmol (g $min^{0.5}$)$^{-1}$ with a rise of about five folds for the increase in PS concentration. Regression values fit well except for the 0.7 mmol L^{-1} and 0.9 mmol L^{-1}.

The Elovich equation is mainly applicable for chemisorption kinetics. The equation is often valid for systems in which the adsorbing surface is heterogeneous [54]. The Elovich model is generally expressed as Eq. (4) where α is the initial adsorption rate (mmol/g min) and β is related to the extent of surface coverage and the activation energy for chemisorption (g/mmol).

$$q_t = \left(\frac{1}{\beta}\right)\ln(\alpha\beta) + \left(\frac{1}{\beta}\right)\ln(t) \tag{4}$$

The plot of q_t vs. ln(t) gives a linear trace with a slope of (1/β) and an intercept of (1/β)ln(αβ). The factor 1/β indicates the number of available sites to accommodate the PS molecules [54] and it was found to exhibit a seven-fold increase from 0.001 to 0.007 g (mmol)$^{-1}$ with respect to three-fold increase in PS concentration. These linear plots are observed with R^2 values between 0.98 and 0.90.

3.7. Adsorption isotherms

The adsorption isotherm is a characteristic representative of the thermodynamic equilibrium between an adsorbent and adsorbate. Using the isotherm models, viz., Langmuir [55], Freundlich [56] and Sips or Langmuir–Freundlich [57] the nature of sorption, sorption capacity and the nature of adsorbent's surface could be explored. The results are represented in Table 2.

The three isotherm parameters are as follows: q_e is quantity of adsorbate (PS) adsorbed per g of adsorbent (mmol g^{-1}); q_{max} is maximum amount of adsorbate to form monolayer (mmol g^{-1}); R_L is dimensionless constant called separation factor; C_e is concentration of the adsorbate in mmol L^{-1}; K_L is Langmuir constant in L (mmol)$^{-1}$; K_F and n are Freundlich constants; K_s is Sips isotherm constant which represents energy of adsorption; and m is empirical constant.

Langmuir adsorption isotherm is an empirical model which assumes a monolayer adsorption (the adsorbed layer is one molecule in thickness) with adsorption occur at a finite number of definite, identical and equivalent localized sites with no lateral interaction and steric hindrance between the adsorbed molecules on adjacent sites [58]. It is referred for homogeneous adsorption, which each molecule possess constant enthalpies and sorption activation energy [59] with no transmigration of the adsorbate in the plane of the surface [60]. The mathematical expression (Eq. (5)) is as follows:

$$q_e = q_{max}\frac{K_L C_e}{1 + K_L C_e} \tag{5}$$

The Langmuir monolayer adsorption capacity was 0.07 mmol g^{-1} and the Langmuir constant was 65.2 L (mg)$^{-1}$. The R^2 value ascertains that this isotherm model fits well with the PS sorption system. R_L values ($R_L = 1 / 1 + K_L C_0$) for the initial PS concentrations (C_0) were calculated in the range 0.017–0.048 with a confirmation that the sorption of PS onto $AlPO_4$ is favorable and likely to be governed by chemical forces as evidenced by the regression value of 0.97 by the Langmuir isotherm.

Freundlich isotherm is an empirical model can be applied to multilayer adsorption over heterogeneous surfaces with non-uniform distribution of adsorption heat and affinities [61]. In this perspective, the amount adsorbed is the summation of adsorption on all sites (each having bond energy), with the stronger binding sites are occupied first, until adsorption energy undergoes an exponential decrease upon the completion of adsorption process [62]. The mathematical expression (Eq. (6)) is as follows:

$$q_e = K_F C_e^{1/n} \tag{6}$$

The slope value (n) range between 0 and 1 is a tool to measure adsorption intensity or surface heterogeneity and becomes more heterogeneous when the value of "n" is close to zero. The value of "n" determined from PS sorption onto $AlPO_4$ indicates the surface heterogeneity value of 0.44.

Table 2
Langmuir, Freundlich and Sips isotherm model parameters for the adsorption of PS onto $AlPO_4$

$q_{max,exp}$ (mmol/g)	Langmuir model			Freundlich model			Sips model			
	$q_{max.cal}$ (mmol/g)	K_L (L/mg)	R^2	K_F (mmol/g)	n	R^2	$q_{max.cal}$ (mmol/g)	K_S (L/mg)	m	R^2
0.063	0.07	65.20	0.97	0.212	0.44	0.89	0.065	0.95	1.34	0.98

The value of 1/n indicates that the sorption is co-operative as the value calculated to be 2.27. The Freundlich PS adsorption capacity of 0.212 mmol g^{-1} was determined with regression value of 0.89 less than that of the Langmuir isotherm model. Thus, the validity of Langmuir is well acknowledged than for the Freundlich isotherm model.

Sips or Langmuir–Freundlich isotherm is a combined form of Langmuir and Freundlich expressions, which predicts the heterogeneous adsorption systems [63] and circumvents the limitation of the rising adsorbate concentration associated with Freundlich isotherm model. Sips isotherm (Eq. (7)), at low adsorbate concentrations, behaves as a Freundlich isotherm; while at high concentrations, it has a characteristic of Langmuir isotherm.

$$q_e = \frac{q_{\max(K_S C_e)^m}}{1+(K_S C_e)^m} \quad (7)$$

The Sips maximum adsorption capacity (q_{max}), Sips equilibrium constant (K_s) and Sips model exponent (m) were determined to be 0.065 mmol g^{-1}, 0.95 L (mg^{-1}) and 1.34, respectively. The Sips isotherm reveals the possibility of adsorption ($m > 1$) on a heterogeneous surface with "m" value equal to 1.34 and indicates more of Freundlich rather than Langmuir. The non-linear fitting (Fig. 7) of the data, obtained for the adsorption of PS onto $AlPO_4$, among the three isotherm models ensures that the linearity of the Sips isotherm model (R^2 = 0.98) was higher than the other two isotherm models (Table 2).

3.8. Comparative analysis of $AlPO_4$ with other adsorbents

The removal of PS by various adsorbents with different surface areas are gathered in Table 3 and compared with the present work. From these results, it appears that the PS adsorption depends on the pH solution and the used technique.

3.9. Desorption studies

The results are presented in (Fig. 8(a)) and show an integral type of desorption curves for both the PS concentrations

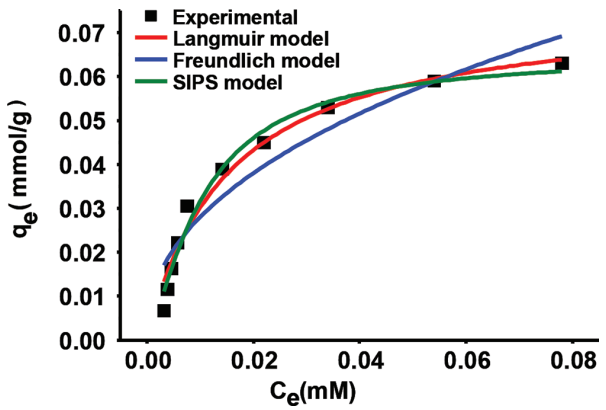

Fig. 7. Langmuir, Freundlich and Sips models of PS adsorption onto 0.2 g of $AlPO_4$ at pH 2.55; T = 22 ± 1°C.

Table 3
Comparative study on PS sorption onto $AlPO_4$ with other adsorbents

Adsorbent material	pH	Specific area (m^2/g)	Adsorption maximal capacity (mg/g) at 25°C	Reference
PVA@SiO1.5-hPEA-1/2Gel	–	–	4,256	[27]
Charcoal ash	2.0	7.45	178.3	[29]
MgO nanoparticles	7.0	22.1	91.3	[28]
$AlPO_4$	2.55	100	47.9	This work
Nb_2O_5	8.0	14	41.0	[23]
Chitin	3.5		05.2	[30]

of 0.03 mM and 0.05 mM. At a pH range of 2.55–4.0, a low desorption was recorded for both the concentrations and the difference between those concentrations was less than 1 μM. Then, the quantity of PS desorption increases from pH 4 and attains a maximum desorption at pH 6. The desorption quantity of PS from pH 6 tends to be constant until it reaches pH 8 with 7 μM and 12 μM, respectively, for 0.03 mM and 0.05 mM PS concentrations. Unlike the poor difference at low pH values, there was an appreciable difference of about 5 μM between PS concentrations in the pH range 6–8. Fig. 8(b) shows a complete desorption of PS at pH 7 from the PS laden $AlPO_4$ surface for two initial solutions of 0.03 and 0.05 mM PS. The initial PS desorption of almost 90% attained rapidly within the first 5 min followed by a constancy of desorption for both the PS concentrations.

3.10. Adsorption on the regenerated adsorbents

Treatment of the PS loaded $AlPO_4$ in a neutral solution resulted in desorption of PS between 86% and 97%. After the PS desorption, the solid was washed three times with a de-ionized water, dried at 80°C and was used for the next adsorption process. The Fig. 9(a) shows the PS adsorption onto the regenerated $AlPO_4$ from PS concentrations (0.03 mM and 0.05 mM). At 50 min of equilibrium time, the rate constant was 1.55 g $(mmol.min)^{-1}$ and 3.71 g $(mmol.min)^{-1}$ for 0.03 and 0.05 mM PS, respectively. These values are close to those found for the fresh (non-regenerated) $AlPO_4$. The color of PS laden $AlPO_4$ appeared red but on thermal treatment by heating at 600°C for 30 min, a white solid was obtained and used for the following adsorption (Fig. 9(b)). The adsorption of the regenerated PS by calcination was also conducted with 0.03 mM and 0.05 mM PS (Fig. 9(b)). The rapid attainment of equilibrium was achievable at the end of 8 min and ascertained that a faster adsorption than that with the original $AlPO_4$ adsorbent. The amount of PS adsorbed onto $AlPO_4$ at equilibrium was 0.0074 mmol g^{-1} and 0.0124 mmol g^{-1}, respectively, at 0.03 mM and 0.05 mM of PS concentration. These values were higher by 0.0007 mmol g^{-1} (0.03 mM) and 0.0009 mmol g^{-1} (0.05 mM) as compared with those of the fresh and non-regenerated $AlPO_4$. Fig. 10 shows

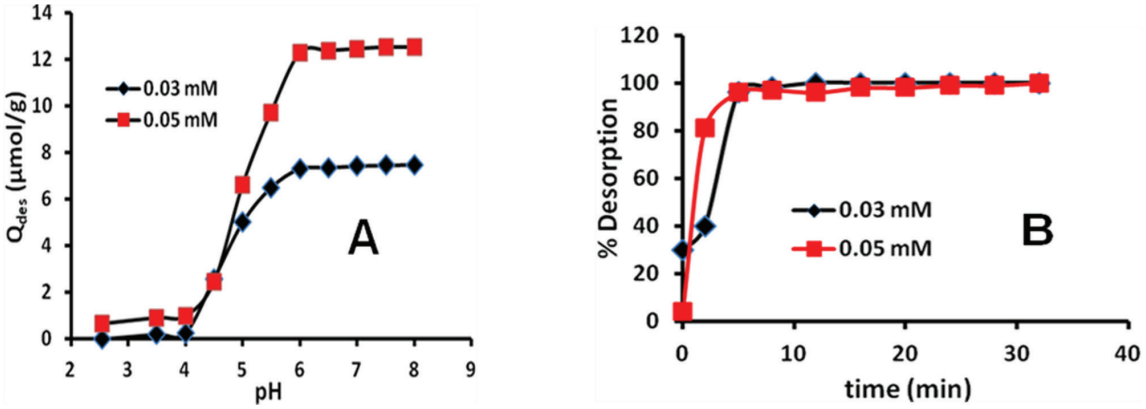

Fig. 8. (a) pH effect of PS desorption from $AlPO_4$ adsorbent at 0.03 mM and 0.05 mM initial concentration, stirring speed = 200 rpm; T = 22 ± 1°C; (b) kinetics desorption of PS initially adsorbed on $AlPO_4$ at pH 7; T = 22 ± 1°C.

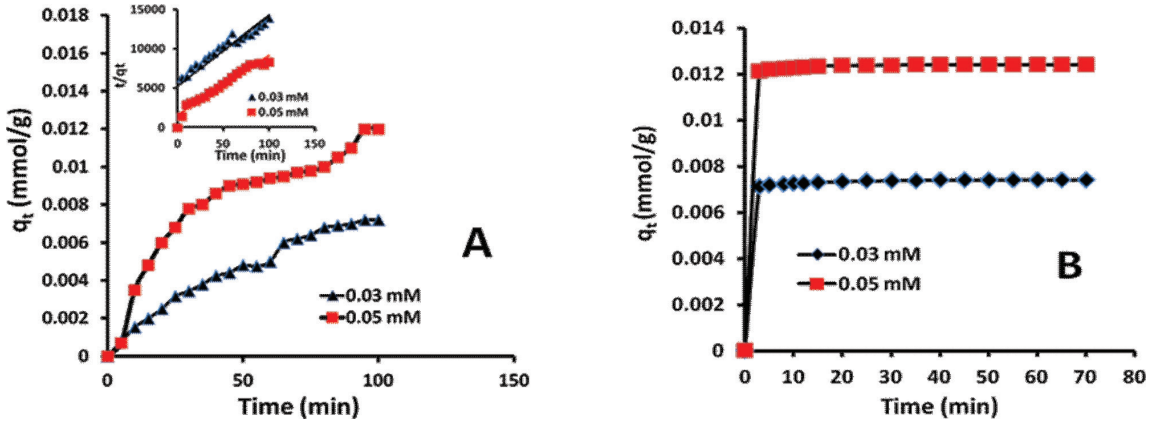

Fig. 9. (a) Adsorption kinetic of PS and pseudo-second-order model onto $AlPO_4$ (regenerated by desorption at pH 7) at pH 2.55 and T = 22 ± 1°C; (b) adsorption kinetics of PS onto 0.2 g of $AlPO_4$ (regenerated by calcinations) at pH 2.55; T = 22 ± 1°C.

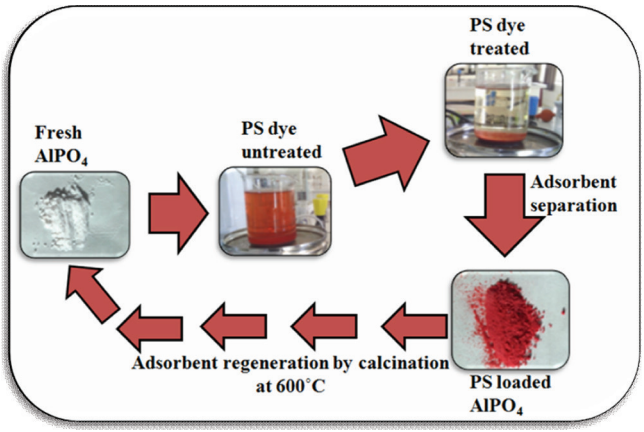

Fig. 10. The recycling process of PS adsorption – desorption – regeneration system.

a summary of the work, treating a solution containing the PS by AlPO4 not regenerated. After equilibrium, the solution is separated by filtration and the solid is treated at neutral pH or by calcination. The solid recovered without PS is newly used for the treatment of another solution containing the PS.

4. Conclusion

The XRD and IR spectral analysis of $AlPO_4$ inferred an amorphous structure and functional group elements, respectively. The pseudo-first-order describes the adsorption of PS onto $AlPO_4$ much better than the other kinetic models. Among the adsorption isotherms, Sips model was approved fit for the present PS sorption system. An exothermic nature of PS sorption onto $AlPO_4$ was well evidenced during the influence of temperature. The washing of followed by thermal regeneration at 600°C for 30 min of PS laden $AlPO_4$ was plausibly achieved. The increase in PS adsorption capacity of regenerated PS was interesting as compared with the fresh (non-regenerated) $AlPO_4$.

References

[1] E. Forgacs, T. Cserhati, G. Oros, Removal of synthetic dyes from wastewaters: a review, Environ. Int., 30 (2004) 953–971.
[2] H.S. Rai, M.S. Bhattacharyya, J. Singh, T.K. Bansal, P. Vats, U.C. Banerjee, Removal of dyes from the effluent of textile and dyestuff manufacturing industry: a review of emerging techniques with reference to biological treatment, Crit. Rev. Env. Sci. Technol., 35 (2005) 219–238.
[3] E.R.A. Ferraz, M.D. Grando, D.P. Oliveira, The azo dye Disperse orange 1 induces DNA damage and cytotoxic effects but does not cause ecotoxic effects in daphnia similis and vibrio fischeri, J. Hazard. Mater., 192 (2011) 628–633.

[4] K.T. Chung, S.E.J. Stevens, C.E. Cerniglia, The reduction of azo dyes by the intestinal microflora, Crit. Rev. Microbiol., 18 (1992) 175–190.
[5] B.N. Ames, J. McCann, E. Yamasaki, Methods for detecting carcinogens and mutagens with the Salmonella/mammalian microsome mutagenicity test, Mutat. Res., 31 (1975) 347–364.
[6] S.W. Oh, M.N. Kang, M.W. Cho, M.W. Lee, Detection of carcinogenic amines from dyestuffs or dyed substrates, Dyes Pigment., 33 (1997) 119–135.
[7] O. Tunay, I. Kabdasli, D. Ohron, G. Cansever, Use and minimalization of water in leather tanning processes, Water Sci. Technol., 40 (1999) 237–244.
[8] S.V. Bannur, S.V. Kulgod, S.S. Metkar, S.K. Mahajan, J.K. Sainis, Protein determination by Ponceau S using digital color image analysis of protein spots on nitrocellulose membranes, Analyt. Biochem., 267 (1999) 382–389.
[9] S.D. Marathe, V.S. Shrivastava, Photocatalytic removal of hazardous Ponceau S dye using nano structured Ni-doped TiO_2 thin film prepared by chemical method, Appl. Nanosci., 5 (2015) 229–234.
[10] A.Y. Zahrim, C. Tizaoui, N. Hilal, Coagulation with polymers for nanofiltration pre-treatment of highly concentrated dyes: a review, Desalination, 266 (2011) 1–16.
[11] F. Zidane, P. Drogui, B. Lekhlif, J. Bensaid, J.-F. Blais, S. Belcadi, K. El-Kacemi, Decolourization of dye-containing effluent using mineral coagulants produced by electrocoagulation, J. Hazard. Mater., 155 (2008) 153–163.
[12] R. Khosravi, S. Hazrati, M. Fazlzadeh, Decolorization of AR18 dye solution by electrocoagulation: sludge production and electrode loss in different current densities, Desalin. Water Treat., 57 (2016) 14656–14664.
[13] Q. Zhuo, H. Ma, B. Wang, L. Gu, Catalytic decolorization of azo-stuff with electro-coagulation method assisted by cobalt phosphomolybdate modified kaolin, J. Hazard. Mater., 142 (2007) 81–87.
[14] K.M. Kodam, I. Soojhawon, P.D. Lokhande, K.R. Gawai, Microbial decolorization of reactive azo dyes under aerobic conditions, World J. Microbiol. Biotechnol., 21 (2005) 367–370.
[15] H.N. Bhatti, S. Noreen, N. Tahir, S. Ilyas, U.H. Siddiqua, Equilibrium, thermodynamic and kinetic studies for biosorption of terasil Brown 2RFL from contaminated water using economical biomaterial, Mediterr. J. Chem., 4 (2015) 239–251.
[16] M. Bouraada, M. Lafjah, M.S. Ouali, L.C.D. Menorval, Basic dye removal from aqueous solutions by dodecylsulfate and dodecyl benzene sulfonate-intercalated hydrotalcite, J. Hazard. Mater., 153 (2008) 911–918.
[17] M.K. Sahoo, L. Sayoo, D.B. Naik, R.N. Sharan, Improving the operational parameters with high electrical energy efficiency for UVC induced advanced oxidation and mineralization of Acid blue 29: generation of eco-friendly effluent, Sep. Purif. Technol., 106 (2013) 110–116.
[18] F.D. Natale, A. Erto, A. Lancia, D. Musmarra, Equilibrium and dynamic study on hexavalent chromium adsorption onto activated carbon, J. Hazard. Mater., 281 (2015) 47–55.
[19] R.C. Meena, R.B. Pachwarya, V.K. Meena, S. Arya, Degradation of textile dyes Ponceau S and Sudan IV using recently developed photocatalyst, immobilized resin Dowex-11, Am. J. Environ Sci., 5 (2009) 444–450.
[20] S.D. Marathe, V.S. Shrivastava, Removal of hazardous Ponceau S dye from industrial wastewater using nano-sized ZnO, Desalin. Water Treat., 54 (2015) 2036–2040.
[21] H.-J. Shin, H.-H. Chae, Removal of Ponceau S from aqueous solutions by organic clay, J. Biosci. Bioeng., 108 (2009) S85–S86.
[22] H.S. El-Desoky, M.M. Ghoneim, N.M. Zidan, Decolorization and degradation of Ponceau S azo-dye in aqueous solutions by the electrochemical advanced Fenton oxidation, Desalination, 264 (2010) 143–150.
[23] B.N. Patil, D.B. Naik, V.S. Shrivastava, Photocatalytic degradation of hazardous Ponceau S dye from industrial wastewater using nanosized niobium pentoxide with carbon, Desalination, 269 (2011) 276–283.
[24] M. Muslim, M.A. Habib, A.J. Mahmood, T.S.A. Islam, I.M.I. Ismail, Zinc oxide-mediated photocatalytic decolorization of Ponceau S in aqueous suspension by visible light, Int. Nano Lett., 30 (2012) 2–9.
[25] M.K. Sahoo, M. Marbaniang, B. Sinha, D.B. Naik, R.N. Sharan, UVC induced TOC removal studies of Ponceau S in the presence of oxidants: evaluation of electrical energy efficiency and assessment of biotoxicity of the treated solutions by Escherichia coli colony forming unit assay, Chem. Eng. J., 213 (2012) 142–149.
[26] M.K. Sahoo, M. Marbaniang, B. Sinha, R.N. Sharan, Fenton and fenton-like processes for the mineralization of Ponceau S in aqueous solution: assessment of eco-toxicological effect of post treated solutions, Sep. Purif. Technol., 124 (2014) 155–162.
[27] S. Deng, H. Xu, X. Jiang, J. Yin, Poly (vinyl alcohol) (PVA)-enhanced hybrid hydrogels of hyper branched poly (ether amine) (hPEA) for selective adsorption and separation of dyes, Macromolecules, 46 (2013) 2399–2406.
[28] T.G. Venkatesha, Y.A. Nayaka, B.K. Chethana, Adsorption of Ponceau S from aqueous solution by MgO nanoparticles, Appl. Surf. Sci., 276 (2013) 620–627.
[29] I. Özbay, U. Özdemir, B. Özbay, S. Veli, Kinetic thermodynamic and equilibrium studies for adsorption of azo reactive dye onto a novel waste adsorbent: charcoal ash, Desalin. Water Treat., 51 (2013) 6091–6100.
[30] D.S. Shirsath, V.S. Shrivastava, Removal of hazardous dye Ponceau S by using chitin: an organic bioadsorbent, Afr. J. Environ. Sci. Technol., 6 (2012) 115–124.
[31] J. Kaur, M. Sharma, O.P. Pandey, Effect of pH on size of ZnS nanoparticles and its application for dye degradation, Particulate Sci. Technol. Inter. J., 33 (2015) 184–188.
[32] M.H. Vijaykumar, P.A. Vaishamapayan, Y.S. Shouche, T.B. Karegoudar, Decolourization of naphthalene-containing sulfonated azo-dyes by kerstersia sp. strain VKY1, Enzyme Microb. Technol., 40 (2007) 204–211.
[33] H. Chen, R.F. Wang, C.E. Cerniglia, Molecular cloning, over expression, purification, and characterization of an aerobic FMN-dependent azo-reductase from Enterococcus faecalis, Protein Expr. Purif., 34 (2004) 302–310.
[34] I. Oller, S. Malato, J.A. Sánchez-Pérez, Combination of advanced oxidation processes and biological treatments for wastewater decontamination—a review, Sci. Total Environ., 409 (2011) 4141–4166.
[35] M.K. Sahoo, M. Marbaniang, B. Sinha, D.B. Naik, R.N. Sharan, UVC induced TOC removal studies of Ponceau S in the presence of oxidants: evaluation of electrical energy efficiency and assessment of biotoxicity of the treated solutions by escherichia coli colony forming unit assay, Chem. Eng. J., 213 (2012) 142–149.
[36] G. Sharma, M. Naushad, D. Pathania, A. Mittal, G.E. El-desoky, Modification of Hibiscus cannabinus fiber by graft copolymerization: application for dye removal, Desalin. Water Treat., 54 (2015) 3114–3121.
[37] S.M. Ahmed, A.A. El-Zomrawy, A.S.N. Al-Kamali, K.A.S. Ghaleb, Ponceau 6R dye decolorization and chromate reduction simultaneously in acid medium, Arab J. Chem., 8 (2015) 500–505.
[38] G. Li, Z. Zhu, B. Qi, G. Liu, P. Wu, G. Zeng, Y. Zhang, et al., Rapid capture of Ponceau S via a hierarchial organic–inorganic hybrid nanofibrous membrane, J. Mater. Chem. A, 4 (2016) 5423–5427.
[39] J. Hu, R. Xu, Rich structure chemistry in the alumino-phosphate family, Acc. Chem. Res., 36 (2003) 481–490.
[40] A. Flilissa, P. Méléard, A. Darchen, Cetylpyridinium removal using phosphate-assisted electrocoagulation, electroreduction and adsorption on electrogenerated sorbents, Chem. Eng. J., 284 (2016) 823–830.
[41] O. Ouariach, M. Kacimi, M. Ziyad, Surface reactivity and self-oscillating oxidation of butan-2-ol over palladium loaded $AlPO_4$, Appl. Catal., A, 503 (2015) 84–93.
[42] G. Newcombe, R. Hayes, M. Drikas, Granular activated carbon: importance of surface properties in the adsorption of naturally occurring organics, Colloids Surf., A: Physicochem. Eng. Asp., 78 (1993) 65–71.
[43] R.H.P. Devamani, M. Alagar, Synthesis and characterization of aluminum phosphate nanoparticles, Int. J. Appl. Sci. Eng. Res., 1 (2012) 769–775.

[44] S. Mustafa, M. Javid, M.I. Zaman, Effect of activation on the sorption properties of $AlPO_4$, Sep. Sci. Technol., 41 (2006) 3467–3484.
[45] Z.G. Zhu, G.H. Li, G.F. Zeng, X.Q. Chen, D. Hu, Y.F. Zhang, Y.H. Sun, Fast capture of methyl-dyes over hierarchical amino-$Co_{0.3}Ni_{0.7}Fe_2O_4$@SiO_2 nanofibrous membrane, J. Mater. Chem. A, 3 (2015) 22000–22004.
[46] X. Fang, S.L. Xiao, M.W. Shen, R. Guo, S.Y. Wang, X.Y. Shi, Fabrication and characterization of water-stable electrospun polyethyleneimine/polyvinyl alcohol nanofibers with super dye sorption capability, New J. Chem., 35 (2011) 360–368.
[47] J.J. Yan, Y.P. Huang, Y.E. Miao, W.W. Tjiu, T.X. Liu, Polydopamine-coated electrospun poly(vinyl alcohol)/poly(acrylic acid) membranes as efficient dye adsorbent with good recyclability, J. Hazard. Mater., 283 (2015) 730–739.
[48] M. Abbas, M. Trari, Kinetic, equilibrium and thermodynamic study on the removal Congo Red from aqueous solutions by adsorption onto apricot stone, Process Saf. Environ. Prot., 98 (2015) 424–436.
[49] K. Zhu, X. Gong, D. He, B. Li, D. Ji, P. Li, Z. Peng, Y. Luo, Adsorption of Ponceau 4R from aqueous solutions using alkali boiled Tilapia fish scales, RSC Adv., 3 (2013) 25221–25230.
[50] S. Lagergren, About the theory of so-called adsorption of soluble substances, der sogenannten adsorption geloster stoffe, K. Svenska Vetenskapsakad. Handl., 24 (1898) 1–39.
[51] Y.S. Ho, G. Mckay, Pseudo-second order model for sorption process, Process Biochem., 24 (1999) 451–455.
[52] W.J. Weber, J.C. Morris, Kinetics of adsorption on carbon from solution, J. Sanit. Eng. Div., Proc. Am. Soc. Civ. Eng., 89 (1963) 31–60.
[53] A.S. Ozcan, B. Erdem, A. Ozcan, Adsorption of acid blue 913 from aqueous solutions onto BTMA-bentonite, Colloid Surf. A., 266 (2005) 73–81.
[54] C. Aharoni, F.C. Tompkins, Kinetics of adsorption and desorption and the Elovich Equation, In: *Advance in catalysis and related subjects*, Academic Press, New York (1970) 1–49.
[55] I. Langmuir, The constitution and fundamental properties of solid and liquid, J. Am. Chem. Soc., 38 (1916) 2221–2295.
[56] H.M.F. Freundlich, Über die adsorption in Lösungen, Z. Phys. Chem., 57 (1906) 385–470.
[57] R. Sips, On the structure of a catalyst surface, J. Chem. Phys., 16 (1948) 490–495.
[58] K. Vijayaraghavan, T.V.N. Padmesh, K. Palanivelu, M. Velan, Biosorption of nickel(II) ions onto Sargassum wightii: application of two-parameter and three parameter isotherm models, J. Hazard. Mater. B, 133 (2006) 304–308.
[59] S. Kundu, A.K. Gupta, Arsenic adsorption onto iron oxide-coated cement (IOCC): regression analysis of equilibrium data with several isotherm models and their optimization, Chem. Eng. J., 122 (2006) 93–106.
[60] A.B. Pérez-Marín, V.M. Zapata, J.F. Ortuno, M. Aguilar, J. Sáez, M. Llorens, Removal of cadmium from aqueous solutions by adsorption onto orange waste, J. Hazard. Mater. B, 139 (2007) 122–131.
[61] A.W. Adamson, A.P. Gast, *Physical chemistry of surfaces*, 6th ed., Wiley Inter Science, New York (1997).
[62] J. Zeldowitsch, Adsorption site energy distribution, Acta. Phys. Chim. URSS, 1 (1934) 961–973.
[63] A. Gunay, E. Arslankaya, I. Tosun, Lead removal from aqueous solution by natural and pretreated clinoptilolite: adsorption equilibrium and kinetics, J. Hazard. Mater., 146 (2007) 362–371.